THE JOURNAL OF PHYSICAL CHEMISTRY B

Article

pubs.acs.org/JPCB

Tetraoctylphosphonium Tetrakis(pentafluorophenyl)borate Room Temperature Ionic Liquid toward Enhanced Physicochemical Properties for Electrochemistry

Tom J. Stockmann and Zhifeng Ding*

Department of Chemistry, The University of Western Ontario, 1151 Richmond Street, London, Ontario, Canada, N6A 5B7

Supporting Information

ABSTRACT: Presented herein is the facile preparation of a new room temperature ionic liquid (RTIL), tetraoctylphosphonium tetrakis(pentafluorophenyl)borate ($P_{8888}TB$). Subsequently, its physicochemical properties such as density, viscosity, and conductivity were characterized relative to temperature, demonstrating values of 1.22 g·cm^{-3}, 727 mPa·s, and 180 μS·cm^{-1}, respectively, at 60 °C. The electrochemistry of $P_{8888}TB$ was also investigated using cyclic voltammetry at a Pt-disk ultramicroelectrode and at a microinterface between water and the RTIL; this analysis revealed a wide metal−electrolyte potential window, ~3.5 V, and a large liquid|liquid polarizable potential window, ~0.9 V, at a temperature of 60 °C. Additionally, electron transfer (ET) reactions at a metal electrode|RTIL interface along with ion transfer (IT) reactions at the water|$P_{8888}TB$ interface were examined; the kinetics of these reactions were explored using finite element analysis. Increased ET and IT kinetics combined with enhancements of physicochemical properties versus RTILs we made previously seemingly suggest modest improvements. However, taken as a whole, they demonstrate significant progress toward a hydrophobic RTIL that can be used in conventional electrochemistry and biphasic metal ion extractions.

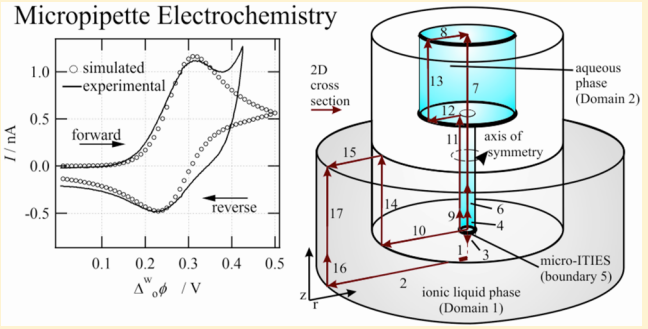

INTRODUCTION

While room temperature ionic liquids (RTILs) are very attractive in conventional electrochemistry, due to their chemical inertness and increased redox potential windows,[1] their applications at the interface between two immiscible electrolytic solutions (ITIES) have been limited because of their hydrophilicity, leading to very narrow potential windows[1,2] and high-cost chemicals.[3,4] We are highly motivated toward the preparation of low-cost RTILs that have enhanced physicochemical properties for electrochemistry.

Since requirements for electrolytes in conventional electrochemistry are very straightforward, we will only emphasize electrochemical aspects at the ITIES. ITIES has been used to study ion transfer reactions between water and 1,2-dichloroethane[2,5−9] (DCE), nitrobenzene (NB),[10,11] as well as trifluorotoluene (TFT);[12] simple ion transfer (IT) can be described using the following:

$$i_w^{z+} \underset{k_b}{\overset{k_f}{\rightleftarrows}} i_o^{z+} \quad (1)$$

whereby ion i with charge $z+$ transfers from aqueous, w, to organic, o. This ion partitioning can be controlled through the application of a potential so that ions can be pushed or pulled across the interface. This facile principle has expanded, resulting in advances toward applications such as sensors,[13,14] ion selective membranes,[15] metal extraction processes,[16−18] along with garnering an improved understanding of ion partitioning and aspects of fundamental electrochemistry.[19−21]

Interestingly, new biphasic solvent combinations are constantly being sought to fulfill the requirements of these burgeoning applications including gels[13,14] and RTILs.[1,2,4,8,16,17,22−25] RTILs are large organic salts often composed of a quaternary alkylammonium/alkylphosphonium or imidazolium cation paired with an asymmetric anion like bis(trifluoromethylsulfonyl)imide ($^-NTf_2$);[2,26] these salts are defined by their low melting point below 100 °C or around room temperature. RTILs have a number of unique properties including low vapor pressure and inherent conductivity and over the past decade have demonstrated themselves to be superior solvents versus traditional organic solvents in biphasic metal ion extraction processes.[16,26] Of particular importance is the extraction of uranium and useful isotopic fission byproducts found in spent nuclear fuel.[16,27,28] These procedures employ a ligand, like tributylphosphate (TBP) used in the plutonium uranium extraction (PUREX)[16] process, dissolved in the organic (or in this case RTIL) phase to coordinate to the metal of interest, making it more miscible to the organic phase. Unfortunately, some of the RTILs tested have demonstrated a disturbing tendency to leach cations through an exchange

Received: August 16, 2012
Revised: September 25, 2012
Published: September 25, 2012

process during metal extraction;[26] an example, using 1-butyl-3-methylimidazolium (C_4mim^+) cation, is detailed below:

$$UO_2^{2+}(aq) + NO_3^-(aq) + TBP(RTIL) + C_4mim^+(RTIL) \rightleftharpoons UO_2NO_3TBP^+(RTIL) + C_4mim^+(aq) \quad (2)$$

In previous organic solvent methods, the uranyl ion coordinates with two nitrate anions forming a neutral species, thus preserving charge neutrality as it partitions to the organic phase.[29] The reaction shown in eq 2 occurs at low aqueous nitric acid concentrations and neutral pH, which are the typical conditions for reclaiming the metal at the end of the extraction procedure.[26] Nevertheless, while RTILs have demonstrated improved extraction efficiency, the leaching of RTIL components during an industrial scale procedure, negating any advantage gained through their nonvolatility, is undesirable for multiple reasons. The primary aim is to recycle these designer solvents during industrial scale use, so losing the cationic component to the aqueous phase is potentially catastrophic for their application.

There are several ways to approach the solution to this problem. One method could be to embrace this deficiency and incorporate a "sacrificial" cation or anion component such that the RTIL could be regenerated during a separate stage at the end of the process.[30] Alternatively, another aqueous ion could be employed to ensure a neutral metal species was formed, as was recently demonstrated by Dietz et al.[31] in their extraction of the pertechnetate anion through the use of a sodium counterion. Lastly, the leaching of cationic or anionic components could be mitigated by simply increasing the hydrophobicity of the RTIL phase.[2,8,26]

This final option is made feasible by augmenting the hydrophobicity of both cations and anions. It is evident that tetrakis(pentafluorophenyl)borate should be an excellent candidate because of its hydrophobicity and chemical inertness.[32,33] While long-chain alkylphosphonium cations do not readily transfer across the ITIES, resulting in very large potential windows,[2,8] tuning physicochemical properties for a better electrochemical performance still needs to be considered. For instance, a cationic/anionic combination should demonstrate the most favorable characteristics of low viscosity, high conductivity, and low melting point, in addition to being extremely hydrophobic. Low cost components are preferred. With these in mind, an extremely hydrophobic RTIL, tetraoctylphosphonium tetrakis(pentafluorophenyl)borate ($P_{8888}TB$), was synthesized. The physicochemical properties such as density, viscosity, and conductivity were analyzed at various temperatures. Electron transfer (ET) and simple ion transfer (IT) reactions at metall RTIL and liquid|liquid interfaces were explored using a Pt-disk ultramicroelectrode (UME) and micro-ITIES housed at the tip of a micropipet (both interfaces were 25 μm in diameter), respectively. Additionally, the kinetics of ET and IT were examined through the use of finite element analysis, which is a computational method for solving nonlinear equations, such as those describing Fick's laws of diffusion and Butler–Volmer equations for charge transfer. The software suite also incorporates the development of two- and even three-dimensional geometries which can be tailored to mirror precisely the experimental apparatus.

SIMULATION STRATEGY

Simulations of electrochemical phenomena have garnered insight into the processes occurring at metal electrode|electrolyte[8,23] and liquid|liquid interfaces.[2,3,7,8,34–36] In particular, finite element analysis can be used to account for the physical geometry of an apparatus, reaction kinetics, as well as exploring their attributes in close relation to the actual experiment.[2,37] Two simulations, electrochemistry at a ultramicroelectrode (UME) and a micro waterlionic liquid interface hosted by a micropipet, were carried out, and their geometries are illustrated in Figure 1A

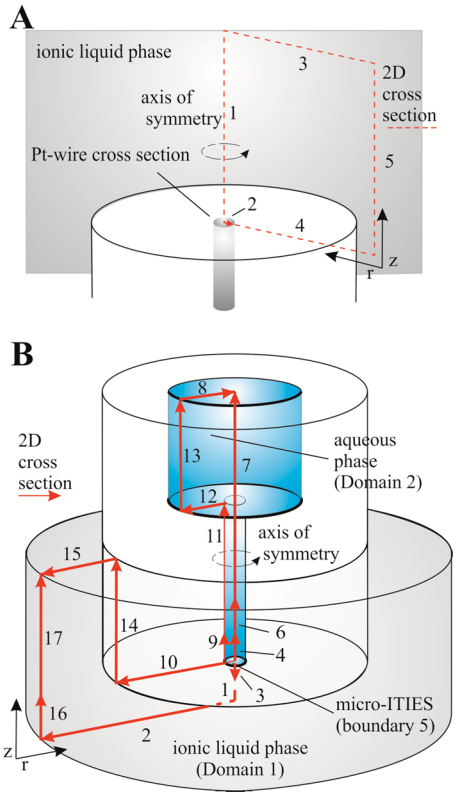

Figure 1. Simulation geometry for (A) the ultramicroelectrode with 2D boundaries (red dashed line) 1, 2, 3, 4, and 5 designated as axial symmetry, flux, concentration, insulator, and concentration, respectively, and (B) the micropipet with the 2D simulation geometry (red arrows) describing the boundary conditions: 5 for flux at the biphasic interface; 1, 3, 4, 6, and 7, axial symmetry; 9–14, insulator (glass surface); 2, 8, 15, 16, and 17, concentration.

and B, respectively. The simulation runtime can be greatly reduced by converting the simulation into its 2D cross section and even further by recognizing the axis of symmetry that still remains. For details, please see the COMSOL reports in the Supporting Information.

The UME geometry (Figure 1A) was composed of five boundaries. The rectangular area framed by these boundaries constitutes the RTIL solution with mass transfer within this area described by Fick's laws of diffusion through eq 3:

$$\frac{\partial c^i(r,z,t)}{\partial t} = D^i\left(\frac{\partial^2 c^i(r,z,t)}{\partial r^2} + \frac{1}{r}\frac{\partial c^i(r,z,t)}{\partial r} + \frac{\partial^2 c^i(r,z,t)}{\partial z^2}\right) = D^i\nabla c^i(r,z,t) = 0 \quad (3)$$

such that c^i and D^i are the concentration and diffusion coefficient of redox species i; ∇, or del, is the gradient or vector operator—

dx.doi.org/10.1021/jp3081832 | J. Phys. Chem. B 2012, 116, 12826–12834

shown here in cylindrical coordinates. The simple one electron oxidation/reduction reaction, as defined by eq 4, was tasked at the electrode surface or boundary 2:

$$\mathrm{Ox} + \mathrm{e}^- \underset{k_b}{\overset{k_f}{\rightleftharpoons}} \mathrm{Red} \tag{4}$$

where the oxidized species, Ox, is reduced to Red through addition of one electron, e^-. The reaction was simulated following Butler−Volmer kinetics represented by eqs 5 and 6 for the forward (k_f) and reverse (k_b) rates:

$$k_f = k^\circ \exp(-\alpha f(E - E^{\circ'})) \tag{5}$$

$$k_b = k^\circ \exp((1 - \alpha) f(E - E^{\circ'})) \tag{6}$$

where k° is the standard rate constant, α is the transfer coefficient (this was assumed to be 0.5 unless otherwise stated), and $f = F/(RT)$, where F is Faraday's constant, R is the universal gas constant, and T is the temperature in Kelvin (taken as 333.15 K or 60 °C). E was the applied potential, and $E^{\circ'}$ was the formal redox potential. Other boundary conditions were set as axial symmetry, concentration, insulator, and concentration for 1, 3, 4, and 5, respectively.

With respect to simulating the liquidlliquid electrochemistry, the geometry can be broken down into two subdomains: domain 1 is for the RTIL phase, while domain 2 represents the aqueous phase. To represent the transfer of a species from one phase (or subdomain) to another required the use of two "diffusion" multiphysics which were each active in one of the two domains and both employed Fick's laws as detailed below in eq 7:

$$\begin{aligned}\frac{\partial c_w^i(r,z,t)}{\partial t} &= D_w^i\left(\frac{\partial^2 c_w^i(r,z,t)}{\partial r^2} + \frac{1}{r}\frac{\partial c_w^i(r,z,t)}{\partial r} + \frac{\partial^2 c_w^i(r,z,t)}{\partial z^2}\right)\\ &= D_w^i \nabla c_w^i(r,z,t)\\ &= 0\end{aligned} \tag{7}$$

In the case of IT, the two domains, water (w) and RTIL, were distinguished through the use of separate diffusion coefficients and by unique concentrations within each subdomain; in this way, eq 7 represents the diffusion of species in subdomain 2, while for subdomain 1 the subscript is simply changed to RTIL. Analogous to the UME simulation, the forward and reverse rate constants k_f and k_b, respectively, detailing IT as shown in eq 1 at the micro-ITIES or boundary 5 (Figure 1B) were treated using Butler−Volmer kinetics through eqs 8 and 9 below:

$$k_f = k^\circ \exp(-\alpha f(\Delta^w_{RTIL}\phi - \Delta^w_{RTIL}\phi^{\circ'})) \tag{8}$$

$$k_b = k^\circ \exp((1 - \alpha) f(\Delta^w_{RTIL}\phi - \Delta^w_{RTIL}\phi^{\circ'})) \tag{9}$$

$\Delta^w_{RTIL}\phi$ is the applied Galvani potential difference across the interface, and $\Delta^w_{RTIL}\phi^{\circ'}$ is the formal transfer potential; $\Delta^w_{RTIL}\phi$ and $\Delta^w_{RTIL}\phi^{\circ'}$ are analogous to E and $E^{\circ'}$ for the ET case.

The other 16 boundaries, as depicted and indicated in Figure 1B, were set as the following: boundaries 2, 8, 15, 16, and 17 had constant concentrations; boundaries 9, 10, 11, 12, 13, and 14 were termed insulators representing the glass surface; and boundaries 1, 3, 4, 6, and 7 composed the axis of symmetry. Boundary 5 was the most critical, as it was tasked as the interfacial surface separating the two phases.

Using the IT simulation as an example, the applied potential profile was a triangular wave function input as a variable into eqs 5, 6, 8, and 9.[38,39]

$$\Delta^w_o\phi = \Delta^w_o\phi_i + \frac{2(\Delta^w_o\phi_f - \Delta^w_o\phi_i)}{\pi} \sin^{-1}\left\{\sin\left[\frac{\pi v t}{2(\Delta^w_o\phi_f - \Delta^w_o\phi_i)}\right]\right\} \tag{10}$$

where $\Delta^w_{RTIL}\phi_i$, $\Delta^w_{RTIL}\phi_f$, v, and t are the initial potential, final potential, scan rate (in $V{\cdot}s^{-1}$), and time. In this way, the potential difference was applied at the interface. The current was integrated at the interface through the following expression:

$$I = 2\pi z_i F \int (-D_\alpha^i \nabla c_\alpha^i(r,z,t)) r \, dr \tag{11}$$

Please note that all simulations were performed in the transient mode which can be switched to steady state within the software suite.

Computations. All simulations were performed using COMSOL Multiphysics 3.5a Software, a finite element analysis platform, using an Acer Aspire Laptop (Acer America Corporation (Canada), Mississauga, ON) equipped with a 1.66 GHz processor and 2 GB of DDR2 RAM; typical simulation runtimes ranged from 3 to 5 min.

EXPERIMENTAL SECTION

Chemicals. All reagents were purchased at the highest quality available and utilized as received without further purification. Trioctylphosphonium, 1-bromooctane, tetramethylammonium sulfate (TMA_2SO_4), tetraethylammonium hydrogen sulfate ($TEAHSO_4$), tetrapropylammonium hydrogen sulfate ($TPrAHSO_4$), tetrabutylammonium hydrogen sulfate ($TBAHSO_4$), lithium sulfate (Li_2SO_4), trioctylphosphine, 1-bromooctane, ferrocene (Fc), bis(pentamethylcyclopentadienyl)iron(II) (or decamethylferrocene, DMFc), 7,7,8,8-tetracyanoquinodimethane (TCNQ), and dichloromethane (DCM) were obtained from Sigma-Aldrich (Sigma-Aldrich Canada, Mississauga, ON). Potassium tetrakis(pentafluorophenyl)borate was bought from Boulder Scientific (Boulder Scientific Company, Longmont, CO). All aqueous solutions were prepared using ultrapure water (18.2 MΩ) processed using a Barnstead water filtration system (Thermo Scientific, Asheville, NC).

Instrumentation. *NMR.* ^{1}H and ^{31}P NMR were acquired by dissolution of ∼7 mg of RTIL sample in $CDCl_3$ and using a 400 MHz Varian Mercury Nuclear Magnetic Resonance Spectrometer.

Conductivity. A Solartron Analytical 1260 Impedance/gain Analyzer (Ametek Advanced Measurement Technology, Farnborough, Hampshire, United Kingdom), along with an electrochemical cell consisting of two disk shaped glassy-carbon electrodes, was employed for the determination of conductivity through the complex impedance method. This method involved scanning the frequency from typically 1 MHz to 300 kHz while monitoring the impedance. A graph of $\log|Z'|$ versus $\log(f)$, where Z' is the real component of the impedance and f is the frequency, reveals an initial plateau followed by a gradual increase; this initial plateau was taken to be a measure of the solution resistance, R_s. A series of KCl solutions of concentrations with known conductivities were prepared and measured. Graphing the known conductivities of these solutions versus $1/R_s$ gives a linear response, that, when fitted using linear

dx.doi.org/10.1021/jp3081832 | J. Phys. Chem. B 2012, 116, 12826−12834

regression, gave a slope of 11.959 cm^{-1}; this slope constitutes the cell constant, l/A, where l is the distance between the two electrodes and A is the electrode area. Using the cell constant, R_s from the ionic liquid sample was measured and translated into conductivity. Temperature within the electrochemical cell was controlled using a water circulator (VWR, Mississauga, ON), while the applied AC voltage amplitude was 0.100 and 1.000 V for the KCl and RTIL solutions, respectively.

Rheometry. The viscosity of $P_{8888}TB$ was determined for various temperatures (controlled by a water circulator) by graphing the shear stress versus shear rate as measured by an AR1500ex Rheometer from TA Instruments (Grimsby, ON); the upper plate diameter and plate gap were 40 mm and 800 μm, respectively.

Density. A DMA4500 Density Meter (Anton Paar, Saint Laurent, Quebec) was used to perform temperature controlled density measurements.

Electrochemistry. Unless otherwise stated, electrochemistry measurements were performed using the Modulab System from Solartron Analytical (Ametek Advanced Measurement Technology, Farnborough, Hampshire, United Kingdom) equipped with a Femto ammeter. All experiments were temperature controlled using a water circulator (VWR, Mississauga, ON) operating at 60 °C unless indicated. Liquidlliquid interfacial experiments utilized a specially prepared micropipet hosted in a modified pipet holder which contained the aqueous phase whereby the micropipet was immersed into the RTIL phase which was kept in a small vial; the interface was maintained at the tip of the capillary and continuously monitored using a CCD camera (Motic Inc., Richmond, BC) with an attached 12× variable zoom lens assembly (Navitar, Rochester, NY). Micropipet and UME fabrication has been described elsewhere.[2,8,16,28] Briefly, a hollow borosilicate glass capillary (1.0 mm/2.0 mm internal/external diameter, Sutter Instrument Co., Novato, CA) was pulled at the center using an electric puller (Narishige, Model #PP-83, Japan). The tapered end of a pulled glass tube was flame annealed. A 1 cm length of 25 μm diameter Pt-wire (Goodfellow Cambridge Ltd., Huntingdon, United Kingdom) was inserted into the cone shape sealing end from the open end. Under reduced pressure, the wire was then annealed in the glass with a sealing length of 1−2 mm by means of the electric puller. The sealed end was subsequently polished to expose the Pt disk and obtain smooth surfaces for both the Pt and glass cross section under a microscope, using a series of grinding/polishing pads (Buehler Canada, Markham, ON). The R_g, the ratio of external diameter (r_g) to internal (a) ($R_g = r_g/a$), was greater than 50. Finally the Pt-wire was etched from the capillary using aqua regia—a 3:1 mixture of HCl:HNO_3. Please note that this leaves a uniform diameter microchannel (~25 μm) which is typically 0.25−0.50 mm in length. The overall capillary length is approximately 5 cm. The pipet tips were then silanized by passing argon gas through the back of the capillary while immersed in a trimethylchlorosilane solution for 5 min. After dry, the capillaries were placed in an oven overnight at 100 °C.

The following electrochemical cells were used:

$$\mathrm{Ag}\,|\,\mathrm{Ag_2SO_4}\,|\,\underset{(aq)}{10\ \mathrm{mM\ Li_2SO_4}}\,\|\,\underset{(RTIL)}{\mathrm{P_{8888}TB}}\,|\,\mathrm{AgTB}\,|\,\mathrm{Ag}\quad \text{Cell 1}$$

$$\mathrm{Ag}\,|\,\mathrm{Ag_2SO_4}\,|\,\underset{(aq)}{\begin{array}{c}5\ \mathrm{mM\ Li_2SO_4}\\ 1\ \mathrm{mM\ LiNO_3}\\ 1\ \mathrm{mM\ NaTPB}\end{array}}\,\|\,\underset{(RTIL)}{\mathrm{P_{8888}TB}}\,|\,\mathrm{AgTB}\,|\,\mathrm{Ag}\quad \text{Cell 2}$$

$$\mathrm{Ag}\,|\,\mathrm{Ag_2SO_4}\,|\,\underset{(aq)}{\begin{array}{c}5\ \mathrm{mM\ Li_2SO_4}\\ 0.5\ \mathrm{mM\ TMA_2SO_4}\\ 1\ \mathrm{mM\ TPAsCl}\end{array}}\,\|\,\underset{(RTIL)}{\mathrm{P_{8888}TB}}\,|\,\mathrm{AgTB}\,|\,\mathrm{Ag}\quad \text{Cell 3}$$

$$\mathrm{Ag}\,|\,\mathrm{Ag_2SO_4}\,|\,\underset{(aq)}{\begin{array}{c}10\ \mathrm{mM\ Li_2SO_4}\\ 0.5\ \mathrm{mM\ TMA_2SO_4}\end{array}}\,\|\,\underset{(RTIL)}{\mathrm{P_{8888}TB}}\,|\,\mathrm{AgTB}\,|\,\mathrm{Ag}\quad \text{Cell 4}$$

$$\mathrm{Ag}\,|\,\mathrm{Ag_2SO_4}\,|\,\underset{(aq)}{\begin{array}{c}10\ \mathrm{mM\ Li_2SO_4}\\ \sim 1\ \mathrm{mM\ XHSO_4}\end{array}}\,\|\,\underset{(RTIL)}{\mathrm{P_{8888}TB}}\,|\,\mathrm{AgTB}\,|\,\mathrm{Ag}\quad \text{Cell 5}$$

RESULTS AND DISCUSSION

$P_{8888}TB$ Preparation and Structural Elucidation. In a glovebox under inert atmospheric conditions, 20 mL (0.045 mol) of trioctylphosphine and 10 mL (0.056 mol) of 1-bromooctane were added to a pressure tube (ACE Glass Inc., Vineland, NJ) along with a magnetic stirrer; the tube was sealed, removed from the glovebox, and stirred for 4 days at room temperature. Subsequently, the pressure tube was opened and charged with 33.2614 g of potassium tetrakis(pentafluorophenyl)borate (KTB) along with 50 mL of dichloromethane (DCM). It is important to note that KTB shows little solubility in DCM; however, its implementation versus a water/methanol mixture ensures that the majority of KBr metathesis product can be removed through filtration; this ultimately results in fewer aqueous−organic extractions during purification. The mixture was stirred for 72 h, after which a white solid, suspended in solution, was removed via Buchner vacuum filtration using #42 ashless filter paper (55 mm in diameter, Little Chalfont, Buckinghamshire, U.K.) beneath an ~1.5 cm thick layer of activated charcoal; DCM was removed under reduced pressure in a rotoevaporator. At this stage, the sample appeared as a viscous, slightly yellow liquid which was dissolved in 125 mL of DCM and extracted 5 times using 125 mL aliquots of ultrapure water.

After removing the DCM, and in order to ensure any unreacted trioctylphosphine was removed, the RTIL was recrystallized in pentane (mp −129 °C) through immersion in a dry ice/acetone bath (−78 °C). In this procedure, a 1:1 volume of pentane to RTIL was combined in a vial and stirred with a glass rod to ensure thorough mixing. This mixture was then placed in the dry ice/acetone bath for 10−15 min at which point the RTIL forms a solid phase at the bottom and the organic solvent can be decanted off the top. This recrystallization was repeated 3 times; the product appears as a soft white solid with a final yield of ~93%.

$P_{8888}TB$ was characterized by proton and phosphorus NMR.

Physicochemical Characterization of $P_{8888}TB$. In order to elucidate its physical properties, the novel RTIL, $P_{8888}TB$, was characterized using a variety of analytical and electrochemical techniques. Figure 2A depicts the cyclic voltammogram (CV) acquired at a scan rate of 0.050 $V{\cdot}s^{-1}$ and at 60 °C using a Pt-disk ultramicroelectrode (UME), 25 μm in diameter. The initial potential started at 0.000 V, and the potential range was between

dx.doi.org/10.1021/jp3081832 | J. Phys. Chem. B 2012, 116, 12826−12834

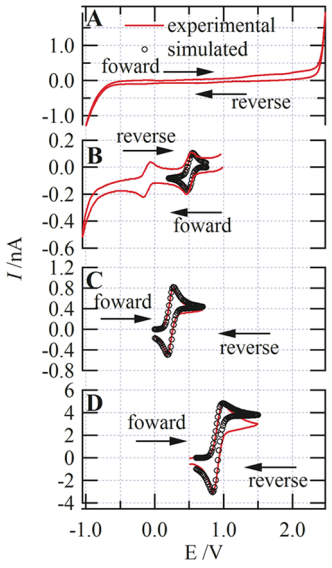

Figure 2. Cyclic voltammograms acquired using a 25 μm Pt-disk ultramicroelectrode with an Ag-wire quasi-reference/counter electrode in $P_{8888}TB$ with (A) no electroactive species, (B) 5 mM TCNQ, (C) 10 mM DMFc, and (D) 17 mM Fc; a scan rate of 0.050 V·s^{-1} was used throughout; (red line) experimental, (○) simulated.

−1.000 and 2.480 V. $P_{8888}TB$ presents a wide metallRTIL potential window, ∼3.5 V, which is similar to our previous ionic liquid, trihexyltetradecylphosphonium tetrakis-(pentafluorophenyl)borate ($P_{66614}TB$),[8] and typical of most RTILs in the literature.[40] The CV shown in Figure 2A highlights the purity of the final RTIL product; the current−potential response is flat within the potential range and free of any peaks caused by impurities. Please note that the potential window might be extended to more negative potentials if the RTIL was degassed (i.e., dissolved O_2 was removed). Subsequently, three electroactive species including 7,7,8,8-tetracyanoquinodimethane (TCNQ), bis(pentamethylpentadienyl)iron(II) (DMFc), and ferrocene (Fc) were dissolved in separate samples of the RTIL and analyzed using CVs.

Figure 2B illustrates the CV obtained with 5 mM TCNQ in $P_{8888}TB$; the scan was initiated at 1.000 V and scanned toward negative potentials at a rate of 0.050 V·s^{-1} until −1.000 V was reached. Two cathodic peaks were observed at 0.461 and −0.160 V corresponding to the reduction of TCNQ to $TCNQ^-$ and, subsequently, $TCNQ^-$ to $TCNQ^{2-}$, respectively. The CV was then scanned into the positive direction from −1.000 to 2.480 V, during which two anodic peaks were observed at −0.070 and 0.524 V which are related to the oxidation of $TCNQ^{2-}$ to $TCNQ^-$ and then $TCNQ^-$ to TCNQ. In fact, the voltammograms depend on the balance between the two processes: diffusion and redox species consumption at the electrode. Owing to the high viscosity in the RTIL, the diffusion is slow, and therefore, electroactive species in the vicinity of the electrode are rapidly consumed. This rapid consumption followed by the slow diffusion of species to the interface generates a peak shaped wave followed by an exponential decay, i.e., a depletion of the species at the electrode. This occurs even when employing UMEs, which typically elicit a steady state current or sigmoidal wave under higher rates of diffusion.[1,8,23,24,41,42]

Interestingly, these two redox couples demonstrate quasi-reversible CV character in that the peak-to-peak separation, ΔE_p, for the TCNQ → $TCNQ^-$ and $TCNQ^-$ → $TCNQ^{2-}$ are 0.063 and 0.060 V, while the ratios of the cathodic to anodic peak currents, $i_{p,c}/i_{p,a}$, are 1.17 and 0.36, respectively; at 60 °C, ΔE_p = 0.066 V and $i_{p,c}/i_{p,a}$ = 1 for a reversible system.[43] It is common that the anodic peak current is different from the cathodic one in RTILs[8,44] owning to a difference in diffusion coefficients[8,41] between the oxidized and reduced state as well as possible solvent relaxation effects.[23] DMFc and Fc were similarly analyzed using $P_{8888}TB$ solutions of 10 and 17 mM and are shown in Figure 2C and D, respectively. The DMFc anodic and cathodic peaks appear at 0.244 and 0.163 V, generating a ΔE_p value of 0.081 V with $i_{p,c}/i_{p,a}$ = 1.00; the Fc redox couple was observed at 1.011/0.866 V, giving values for ΔE_p and $i_{p,c}/i_{p,a}$ of 0.144 V and 1.14, respectively. The response for all three electroactive species show improved reversibility versus the previous RTIL with peak-to-peak separations at or near the desired 0.066 V. Interestingly, the peak current ratios for all species are close to 1, which seems to indicate that the RTIL environment has the same affinity, or degree of intermolecular interaction, for both the reduced and oxidized forms. The $TNCQ^-/TCNQ^{2-}$ couple is the only exception ($i_{p,c}/i_{p,a}$ = 0.36); however, this may be owing to an increased charge localization and therefore an increase in the level of interaction. Through a facile scan rate experiment,[43] the diffusion coefficients were determined for $TCNQ/TCNQ^-$, $DMFc/DMFc^+$, and Fc/Fc^+ to be 2.7, 6.1, and 10.9 × 10^{-8} cm^2·s^{-1}, respectively.

In order to evaluate further the kinetics of electron transfer (ET), simulated CVs were generated through COMSOL 3.5a Multiphysics software employing finite element analysis and overlaid onto experimental curves. These simulations were performed using the geometry depicted in Figure 1A along with Fick's laws of diffusion to govern the mass transfer of species while Butler−Volmer kinetics, at the electrode surface, detailed the oxidation/reduction of the species of interest. Figure 2 illustrates the first redox couple for each of the three electroactive species with the experimental curves (solid line) and simulated curves (○) overlaid. Unlike in conventional electrolyte solutions, RTILs seem to induce a change in the effective diffusion coefficients between two different charge states within a species. This disparity in between the oxidized and reduced states has been recognized by Hapiot's group[42,45] using the redox species like $O_2/O_2^{\bullet-}$ and by Compton et al. through their work with ferrocene and arenes.[23,41] The disparity between the two peak current values can result in a ratio of D_{red}/D_{ox} of up to 1000 times difference.[42] Therefore, for the electroactive species studied here, three parameters were of primary importance for optimiztion: $k°$, D^i_{ox}, and D^i_{red} which are the standard rate constant along with the diffusion coefficient of the oxidized and reduced state, respectively.

Thus, for the $TCNQ/TCNQ^-$ couple, these parameters were optimized at 5 × 10^{-3} cm·s^{-1} for $k°$, while both D_{ox}^{TCNQ} and $D_{red}^{TCNQ^-}$ were set equal to 1.25 × 10^{-8} cm^2·s^{-1}. Similarly, for $DMFc/DMFc^+$, $k°$ was 5 × 10^{-3} cm·s^{-1}, while $D_{ox}^{DMFc^+}$ and D_{red}^{DMFc} were 5.6 and 4 × 10^{-8} cm^2·s^{-1}. The Fc/Fc^+ couple showed slightly different characteristics with a smaller $k°$ value of 5 × 10^{-4} cm·s^{-1} and with a much larger disparity in diffusion coefficients having $D_{ox}^{Fc^+}$ and D_{red}^{Fc} equal to 9 and 4 × 10^{-8} cm^2·s^{-1}. For $TCNQ/TCNQ^-$ and $DMFc/DMFc^+$, the simulation overlay demonstrates excellent agreement with the experimental CV, while that shown for Fc/Fc^+ is relatively good; this indicates the success of the chosen parameters. Please note, however, that the $k°$ values used in the simulation should be considered apparent values.

dx.doi.org/10.1021/jp3081832 | J. Phys. Chem. B 2012, 116, 12826−12834

Interestingly, the ratio of D^{Fc}/D^{Fc^+} and D^{DMFc}/D^{DMFc^+} was 0.44 and 0.70 which is in reasonable agreement with those reported by Compton's group; using a ferrocene redox couple, they detailed a ratio of 1−2 for the majority of RTILs they examined; however, they also reported a value of 7.80 for the RTIL trihexyltetradecylphosphonium trifluorotris(pentafluoroethyl)phosphate (P_{66614}FAP). Additionally, our previous RTIL, P_{66614}TB, showed a similar result compared to Compton et al.[41] with a value of 6.4.[8] It is possible that, because both the cation and anion in P_{8888}TB are highly symmetrical, this reduces the influence of the RTIL environment toward the electroactive species and thus the diffusion coefficients in the present case are close to 1.

Table 1 lists the physical properties of density, viscosity, and conductivity measured over a series of increasing temperatures for pure P_{8888}TB. As expected, the viscosity and density decrease with increasing temperature. The viscosity is high when compared to imidazolium and quaternary ammonium/phosphonium cations[8,24,25] coupled with bis(trifluoromethylsulfonyl)-imide (NTf_2) as an anion; however, it demonstrates a modest decrease relative to our previous RTIL, P_{66614}TB. This is especially true at 60 °C, where P_{66614}TB[8] and P_{8888}TB are 1206 and 727 mPa·s, respectively. A low viscosity is advantageous for RTILs in terms of pour-ability and thus their ease of use. However, in terms of liquid|liquid electrochemistry, a viscous organic phase has been shown to improve the stability of the interface. Similarly, the conductivity of P_{8888}TB is relatively good compared with other ionic liquids[44] and shows a slight improvement versus P_{66614}TB.[8]

Table 1. The Density, Viscosity, and Conductivity Relative to Temperature for the Pure P_{8888}TB RTIL

temp (°C)	density ($g \cdot cm^{-3}$)	viscosity (mPa·s)	conductivity ($\mu S \cdot cm^{-1}$)
25	1.248	7101.11	157.5
35	1.239	3480.17	157.4
45	1.235	1718.39	162.8
50	1.226	1278.39	161.3
60	1.218	726.98	162.0
70	1.209	444.63	180.4
80	1.201	288.53	
90		196.32	

Electrochemistry at Water|P_{8888}TB Microinterfaces. Figure 3 shows a CV acquired using cell 1, or a "blank" CV, at a micro-ITIES housed at the tip of a micropipet with an initial potential of −0.121 V, a potential range from −0.470 to 0.476 V, and a scan rate of 0.020 $V \cdot s^{-1}$. This CV demonstrates the wide polarizable potential window (PPW) available at a w|RTIL interface using P_{8888}TB. The positive end of the PPW is limited by the transfer of the anionic component of the RTIL phase, TB^-, from RTIL to w and Li^+ from w to RTIL. Similarly, the negative end is limited by the transfer of SO_4^{2-} from w to RTIL and the cationic component of the RTIL, P_{8888}^+, from RTIL to w. In this way, the total size of the PPW is ∼0.9 V which is comparable to other w|RTIL systems[3,8,22] but shows marked improvement versus RTILs which incorporate the NTf_2 anion; these are typically limited to a PPW no larger than ∼0.4 V.[2]

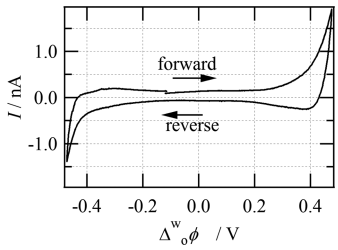

Figure 3. Cyclic voltammogram taken at a w|P_{8888}TB microinterface using cell 1 with an initial potential of −0.121 V, a scan rate of 0.020 $V \cdot s^{-1}$, and a potential range from −0.470 to 0.476.

Analogous to redox chemistry at a UME, IT at a w|RTIL microinterface reveals symmetric character, i.e., a peak shaped current−potential response, in both the forward and reverse directions. At traditional water|organic solvent micropipet interfaces, this is not usually the case. For example, at a w|DCE micropipet ITIES, the CV result is typically asymmetric such that ions crossing from inside to outside the pipet are rapidly consumed owing to the small volume of solution within the microchannel associated with the interface generating a peak shaped wave; this is sometimes called linear diffusion. Those crossing from outside to inside display a sigmoidal or "S" shaped wave owing to the relatively large hemispherical volume directly surrounding the ITIES; this provides a sufficient amount of ions to elicit and maintain a steady state current—often referred to as hemispherical diffusion. Because the RTIL phase outside the capillary is viscose, this leads to a very low diffusion coefficient. The ion transfer rate is faster than the ion transport to the electrode. A peak shaped wave is the result of the ion depletion at the interface. This is also why, at the edge of the PPW, there is a return peak directly after the switching potential.

Liquid|liquid electrochemistry can be used to directly measure the formal transfer potential, $\Delta^w_{RTIL}\phi^{o'}$, of a charged species whereby the formal transfer potential is related to the Gibb's free energy of transfer, analogous to metallelectrolyte interfaces, as $\Delta G_i^{o',RTIL\rightarrow w} = zF\Delta^w_o\phi_i^{o'}$. In this way, using the potentials at the edge of the CV shown in Figure 3 to estimate $\Delta^w_o\phi^{o'}$ of the cationic and anionic components of the RTILs and substituting them into eq 12,[22] which follows, the solubility constant, K^w_{sp}, was approximated as 5.0×10^{-15}.

$$\ln K^w_{sp} = -\frac{zF\Delta^w_{RTIL}\phi^{o'}_{cation} - zF\Delta^w_{RTIL}\phi^{o'}_{anion}}{RT} \quad (12)$$

It was assumed that the ions limiting the PPW were RTIL. The K^w_{sp} given is a "worst case scenario", and it is possible that this value is even lower. Therefore, P_{8888}TB is an extremely hydrophobic RTIL which is critical as the larger the PPW the more electrochemical phenomenon can be observed and recorded. This increase in hydrophobicity translates directly into a decreased propensity to undergo cationic exchange during biphasic, water−RTIL, metal extraction procedures.[26] Dietz et al.[26] discovered that RTILs composed of short chain dialkylimidazolium cations undergo a cationic exchange mechanism at low concentrations of nitric acid in the aqueous phase. This results in the transfer of a charged metal complex, e.g., $UO_2NO_3TBP^+$ (where TBP is the ligand tributylphosphate), into the RTIL phase and, in order to maintain charge neutrality, an imidazolium cation transfers into the aqueous phase; at high nitric acid concentrations (low pH), two nitrate molecules coordinate to the metal center and generate a neutral complex.[26] They also found that increase in the alkyl chain length on the imidazolium could eliminate this from happening, i.e., make the RTIL more hydrophobic. On the basis of the low K^w_{sp} estimated herein for P_{8888}TB, it is likely to conclude that cationic exchange would be negligible.

dx.doi.org/10.1021/jp3081832 | J. Phys. Chem. B 2012, 116, 12826−12834

It is important to mention that NTf_2^- based ionic liquids, while demonstrating favorable physical characteristics like low viscosity and high conductivity, experience PPWs that are too small to be of use in liquidlliquid electrochemistry;[2] therefore, TB^- based RTILs are preferred because they are more hydrophobic, giving access to a much wider liquidlliquid potential range.

Unlike metallelectrolyte interfaces whose potential range can be calibrated using a reference electrode, in liquidlliquid chemistry, the potential is often calibrated with an internal standard according to a nonthermodynamic assumption: the tetraphenylarsonium-tetraphenylborate (TATB) or Parker's assumption.[46] Parker's assumption states that the Gibbs free energies of transfer are equal for tetraphenylarsonium ($TPAs^+$) and tetraphenylborate (TPB^-); since they are of opposite charge, experimentally their IT appears at opposite ends of the PPW and the midpoint between their transfer, captured via CV, is the point of zero charge (PZC).[46] This calibration has been utilized for the interface between water and traditional molecular solvents such as DCE and NB over the past 30 years[4,47−49] and recently for the w|TFT ITIES.[12]

Therefore, employing cells 2 and 3, the CVs of TPB^- and $TPAs^+$ simple IT were recorded and are displayed as an overlay in Figure 4. By using the edge of the PPW to align the CVs, the PZC

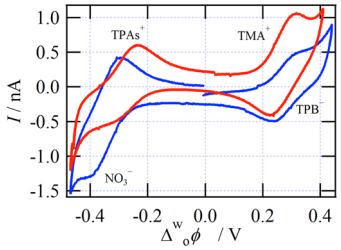

Figure 4. Cyclic voltammograms recorded using cell 2 (blue line) and cell 3 (red line); instrument parameters are similar to those detailed for Figure 2.

and ultimately the formal transfer potential of these two ions was estimated; $\Delta^{w}_{RTIL}\phi^{o'}_{TPB^-}$ and $\Delta^{w}_{RTIL}\phi^{o'}_{TPAs^+}$ were determined to be 0.288 and −0.288 V, respectively. The anodic to cathodic peak separation was improved significantly in reference to the other RTILs prepared by us.[8] An attempt was made to record a CV with both TPB^- and $TPAs^+$ dissolved in the aqueous phase; however, despite hours of sonication, not enough of the TPAsTPB salt was dissolved to appear on a CV. Similarly, dissolving TPAsTPB in $P_{8888}TB$ is problematic, as it seems to undergo metathesis with the RTIL, altering its physical properties.

Simultaneously, the IT of NO_3^- and TMA^+ were also performed, as shown in Figure 4 with formal transfer potentials

Table 2. Formal Transfer Potentials for Ions at the w|$P_{8888}TB$ Interface Based on the TATB Assumption

Ion	$\Delta^{w}_{o}\phi^{o'}$ (V)
$TPAs^+$	−0.288
TMA^+	0.270
TEA^+	0.100
$TPrA^+$	−0.044
TBA^+	−0.179
TPB^-	0.288
NO_3^-	−0.352

determined to be −0.352 and 0.270 V, so that these ions could then be used to calibrate other species IT. Figure 5 demonstrates

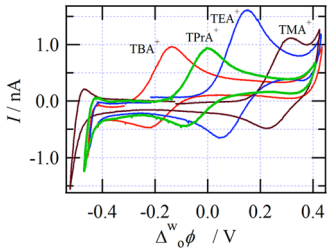

Figure 5. Cyclic voltammograms acquired using cell 4 (brown line) and cell 5 with X = TBA^+ (red line), $TPrA^+$ (green line), and TEA^+ (blue line); the peak currents associated with the simple IT for each species have been labeled correspondingly. Please note that each ion transfer potential has been calibrated using TMA^+ IT according to the TATB assumption.

this using cell 4 for TMA^+ IT as well as cell 5 with X equal to tetraethylammonium (TEA^+), tetrapropylammonium ($TPrA^+$), and tetrabutylammonium (TBA^+), which were all calibrated after addition of 0.8 mM TMA^+ to the cell, and demonstrated formal transfer potentials of 0.100, −0.044, and −0.179 V, respectively. These transfer potentials have been summarized in Table 2. Interestingly, the trend in formal transfer potentials agrees well with that shown at the w|DCE,[5,6] w|NB,[6] and w|TFT,[12] which is similar to that demonstrated recently for an w|RTIL ITIES.[17] That is, with increasing hydrophobicity of the ion, correlated to increasing alkyl chain length in the case of the alkylammonium cations, the formal transfer potentials shift to more negative values, i.e., $TMA^+ > TEA^+ > TPrA^+ > TBA^+$.

Similar to the ET case, IT was explored through simulations with the geometry shown in Figure 1B. Figure 6 depicts the CV

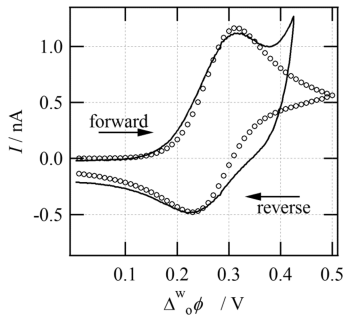

Figure 6. Cyclic voltammograms recorded using cell 4 (solid line) displaying TMA^+ ion transfer along with a simulated curve (○) generated using the geometry shown in Figure 1A.

obtained using cell 4 for TMA^+ transfer (solid line) and with the simulated curve overlaid (○). The key kinetic parameters used to generate the latter were k^o, D_{aq}, D_{org}, and $\Delta^{w}_{o}\phi^{o'}_{TMA^+}$ with optimized values of 2×10^{-3} cm·s^{-1}, 1.8×10^{-5} cm^2·s^{-1}, 1.5×10^{-8} cm^2·s^{-1}, and 0.175 V. Interestingly, based on these values, the kinetics of IT at the w|$P_{8888}TB$ interface are 4 times faster than that shown previously for w|$P_{66614}TB$, where k^o was found to be 5×10^{-4} cm·s^{-1}.

Using this simulation code, the general effect of varying the standard rate constants was also explored and is illustrated in Figure 7 whereby k^o was varied from, at its highest, 1×10^5 to 1×10^{-4} cm·s^{-1}, at the low end; please note that any standard rate constant above 1×10^{-2} cm·s^{-1} elicits overlapping traces which

dx.doi.org/10.1021/jp3081832 | J. Phys. Chem. B 2012, 116, 12826−12834

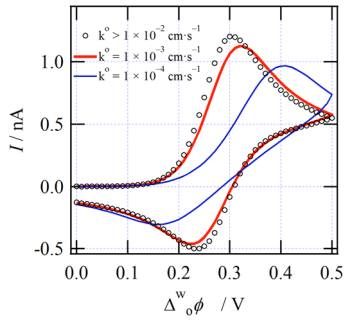

Figure 7. Simulated cyclic voltammograms generated using $k > 1 \times 10^{-2}$ (○) along with 1×10^{-3} (red line) and 1×10^{-4} $cm^2 \cdot s^{-1}$ (blue line).

are consistent with the Butler–Volmer kinetics reaching a Nernstian or completely reversible state. This facile exercise also illustrates that as the standard rate constant is reduced the peak-to-peak separation increases and the system trends toward a quasi-reversible state. Interestingly, the $k°$ optimized herein is almost an order of magnitude greater than that demonstrated by $P_{66614}TB$; therefore, IT at the w|$P_{8888}TB$ interface shows more reversible character.

It is important to note that most $k°$ values reported herein, for both the UME and ITIES cases, lay between 1×10^{-2} and 1×10^{-3} $cm \cdot s^{-1}$, and this agrees well with their peak-to-peak separation values which suggest reversibility, i.e., quasi-reversible trending toward a fully reversible state. These minor changes to the apparent $k°$ are really a consequence of "dialing-in" the simulation, and as can be seen from Figure 7, this term also influences slightly the peak-current response. There is ultimately little change between these two, but a dramatic difference can be seen when the apparent standard rate constant drops from 1×10^{-3} and 1×10^{-4} $cm \cdot s^{-1}$.

CONCLUSIONS

Through a facile synthetic process, a hydrophobic RTIL, $P_{8888}TB$, was prepared using cost-effective starting materials and purified through a simple recrystallization technique. Critically, this RTIL demonstrates a series of modest improvements over previous RTILs including a reduced viscosity, higher conductivity, and more reversible ET and IT kinetics. The characterization of the RTIL was performed through a variety of analytical techniques, while the ET and IT kinetics were developed using a well established finite element analysis or simulation program; this program allows for the development of 2D and 3D geometric models to better approximate experimental conditions.

It is important to note that other RTILs based on imidazolium cations or bis(trifluoromethylsulfonyl)imide anions are not sufficiently hydrophobic to offer a wide PPW at liquidlliquid interfaces. Therefore, while these RTILs may demonstrate more favorable physical characteristics, like conductivity, they are not suitable for ITIES electrochemistry and thus cannot readily be used to investigate IT or ligand assisted ion transfer.

Finally, while the many improvements $P_{8888}TB$ shows over our previous RTIL[8] may be minor when examined individually, taken together they amount to a significant enhancement. Applications of $P_{8888}TB$ in electrochemistry are anticipated.

ASSOCIATED CONTENT

Supporting Information

COMSOL simulation reports for electrochemistry at a microelectrode in ionic liquid and at the water/ionic liquid microinterface. This material is available free of charge via the Internet at http://pubs.acs.org.

AUTHOR INFORMATION

Corresponding Author

*Phone: +1 519 661-2111, ext 86161. Fax: +1 519 661-3022. E-mail: zfding@uwo.ca. URL: http://publish.uwo.ca/~zfding/.

Notes

The authors declare no competing financial interest.

ACKNOWLEDGMENTS

We would like to extend our eternal gratitude to J. Clara Wren, Jamie Noël, David W. Shoesmith, Paul J. Ragogna, Sherrie McPhee, and Marylou Hart for their helpful discussions and technical support. Thanks also to Dr. John de Bruyn for the use of his rheological equipment and Dr. Rick Secco for the use of his impedance analyzer. Special thanks to John Vanstone, Jon Aukima, and Justin Smith in Western Chemistry Departments Electronic Shop for the fabrication/modification of the micropipet holder. We gratefully acknowledge Cytec Inc. for their generous gift of $P_{8888}Cl$ for comparison to our own prepared RTIL. This work was supported by the Ontario Research Fund, Natural Sciences and Engineering Research Council of Canada, Canada Foundation for Innovation, Ontario Innovation Trust, the Premier's Research Excellence Award, and the University of Western Ontario. T.J.S. is grateful to the Queen Elizabeth II Graduate Scholarship in Science and Technology (QEIIGSST).

REFERENCES

(1) Quinn, B. M.; Ding, Z.; Moulton, R.; Bard, A. J. *Langmuir* **2002**, *18*, 1734–1742.
(2) Stockmann, T. J.; Ding, Z. *J. Electroanal. Chem.* **2010**, *649*, 23–31.
(3) Nishi, N.; Murakami, H.; Imakura, S.; Kakiuchi, T. *Anal. Chem.* **2006**, *78*, 5805–5812.
(4) Samec, Z.; Langmaier, J.; Kakiuchi, T. *Pure Appl. Chem.* **2009**, *81*, 1473–1488.
(5) Wandlowski, T.; Marecek, V.; Samec, Z. *Electrochim. Acta* **1990**, *35*, 1173–1175.
(6) Sabela, A.; Mareček, V.; Samec, Z.; Fuoco, R. *Electrochim. Acta* **1992**, *37*, 231–235.
(7) Stockmann, T. J.; Olaya, A. J.; Méndez, M. A.; Girault, H. H.; Ding, Z. *Electroanalysis* **2011**, *23*, 2677–2686.
(8) Stockmann, T. J.; Zhang, J.; Wren, J. C.; Ding, Z. *Electrochim. Acta* **2012**, *62*, 8–18.
(9) Cui, R. F.; Li, Q.; Gross, D. E.; Meng, X.; Li, B.; Marquez, M.; Yang, R. H.; Sessler, J. L.; Shao, Y. H. *J. Am. Chem. Soc.* **2008**, *130*, 14364–14365.
(10) Satoh, M.; Aoki, K.; Chen, J. *Langmuir* **2008**, *24*, 4364–4369.
(11) Li, M.; Aoki, K.; Chen, J.; Nishiumi, T. *J. Electroanal. Chem.* **2011**, *655*, 159–163.
(12) Olaya, A. J.; Ge, P.; Girault, H. H. *Electrochem. Commun.* **2012**, *19*, 101–104.
(13) Faisal, S. N.; Pereira, C. M.; Rho, S.; Lee, H. J. *Phys. Chem. Chem. Phys.* **2010**, *12*, 15184–15189.
(14) Hossain, M. M.; Girault, H. H.; Lee, H. J. *Bull. Korean Chem. Soc.* **2012**, *33*, 1734–1740.
(15) Langmaier, J.; Samec, Z. *Anal. Chem.* **2009**, *81*, 6382–6389.
(16) Stockmann, T. J.; Ding, Z. *Anal. Chem.* **2011**, *83*, 7542–7549.
(17) Langmaier, J.; Trojanek, A.; Samec, Z. *Electroanalysis* **2009**, *21*, 1977–1983.

(18) Stockmann, T. J.; Lu, Y.; Zhang, J.; Girault, H. H.; Ding, Z. *Chem.—Eur. J.* **2011**, *17*, 13206−13216.
(19) Partovi, N. R.; Su, B.; Mendez, M. A.; Barbe, J.-M.; Samec, Z.; Girault, H. H. *J. Electroanal. Chem.* **2011**, *656*, 147−151.
(20) Sun, P.; Li, F.; Chen, Y.; Zhang, M. Q.; Zhang, Z. Q.; Gao, Z.; Shao, Y. H. *J. Am. Chem. Soc.* **2003**, *125*, 9600−9601.
(21) Partovi-Nia, R.; Su, B.; Méndez, M. A.; Habermeyer, B.; Gros, C. P.; Barbe, J.-M.; Samec, Z.; Girault, H. H. *ChemPhysChem* **2010**, *11*, 2979−2984.
(22) Kakiuchi, T. *Anal. Chem.* **2007**, *79*, 6442−6449.
(23) Belding, S. R.; Rees, N. V.; Aldous, L.; Hardacre, C.; Compton, R. G. *J. Phys. Chem. C* **2008**, *112*, 1650−1657.
(24) Barrosse-Antle, L. E.; Hardacre, C.; Compton, R. G. *J. Phys. Chem. B* **2009**, *113*, 2805−2809.
(25) Nishi, N.; Suzuki, A.; Kakiuchi, T. *Bull. Chem. Soc. Jpn.* **2009**, *82*, 86−92.
(26) Dietz, M. L.; Stepinski, D. C. *Talanta* **2008**, *75*, 598−603.
(27) Bruno, J.; Ewing, R. C. *Elements* **2006**, *2*, 343−349.
(28) Stockmann, T. J.; Montgomery, A.-M.; Ding, Z. *Anal. Chem.* **2012**, *84*, 6143−6149.
(29) Nash, K. L. In *Separations for the Nuclear Fuel Cycle in the 21st Century*; Lumetta, G. J., Nash, K. L., Clark, S., B., Friese, J. I., Eds.; American Chemical Society: Washington, DC, 2006; pp 22−40.
(30) Luo, H.; Dai, S.; Bonnesen, P. V.; Buchanan, A. C.; Holbrey, J. D.; Bridges, N. J.; Rogers, R. D. *Anal. Chem.* **2004**, *76*, 3078−3083.
(31) Stepinski, D. C.; Vandegrift, G. F.; Shkrob, I. A.; Wishart, J. F.; Kerr, K.; Dietz, M. L.; Qadah, D. T. D.; Garvey, S. L. *Ind. Eng. Chem. Res.* **2010**, *49*, 5863−5868.
(32) Fermin, D. J.; Dung, D. H.; Ding, Z.; Brevet, P. F.; Girault, H. H. *Phys. Chem. Chem. Phys.* **1999**, *1*, 1461−1467.
(33) Brown, A. R.; Yellowlees, L. J.; Girault, H. *J. Chem. Soc., Faraday Trans.* **1993**, *89*, 207−212.
(34) Zhao, C.; Bond, A. M.; Compton, R. G.; O'Mahony, A. M.; Rogers, E. I. *Anal. Chem.* **2010**, *82*, 3856−3861.
(35) Zhurov, K.; Dickinson, E. J. F.; Compton, R. G. *J. Phys. Chem. B* **2011**, *115*, 12429−12440.
(36) Deryabina, M. A.; Hansen, S. H.; Jensen, H. *Anal. Chem.* **2011**, *83*, 7388−7393.
(37) Josserand, J.; Morandini, J.; Lee, H. J.; Ferrigno, R.; Girault, H. H. *J. Electroanal. Chem.* **1999**, *468*, 42−52.
(38) Rodgers, P. J.; Amemiya, S. *Anal. Chem.* **2007**, *79*, 9276−9285.
(39) Wang, Y.; Velmurugan, J.; Mirkin, M. V.; Rodgers, P. J.; Kim, J.; Amemiya, S. *Anal. Chem.* **2010**, *82*, 77−83.
(40) Wu, T.-Y.; Su, S.-G.; Lin, Y.-C.; Wang, H. P.; Lin, M.-W.; Gung, S.-T.; Sun, I. W. *Electrochim. Acta* **2010**, *56*, 853−862.
(41) Rogers, E. I.; Silvester, D. S.; Poole, D. L.; Aldous, L.; Hardacre, C.; Compton, R. G. *J. Phys. Chem. C* **2008**, *112*, 2729−2735.
(42) Zigah, D.; Wang, A.; Lagrost, C.; Hapiot, P. *J. Phys. Chem. B* **2009**, *113*, 2019−2023.
(43) Bard, A. J.; Faulkner, L. R. *Electrochemical Methods: Fundamentals and Applications*, 2nd ed.; John Wiley: New York, 2001.
(44) Lu, X.; Burrell, G.; Separovic, F.; Zhao, C. *J. Phys. Chem. B* **2012**, *116*, 9160−9170.
(45) Ghilane, J.; Lagrost, C.; Hapiot, P. *Anal. Chem.* **2007**, *79*, 7383−7391.
(46) Parker, A. J. *Electrochim. Acta* **1976**, *21*, 671−679.
(47) Molina, A.; Serna, C.; Ortuno, J. A.; Torralba, E. *Annu. Rep. Prog. Chem., Sect. C: Phys. Chem.* **2012**, *108*, 126−176.
(48) Girault, H. H. J.; Schiffrin, D. J. In *Electroanalytical Chemistry*; Bard, A. J., Ed.; Marcel Dekker: New York, 1989; Vol. *15*, pp 1−141.
(49) Girault, H. *Analytical and Physical Electrochemistry*, 1st ed.; EPFL Press: Lausanne, CH, 2004.